A short-chain multi-branched perfluoroalkyl thiol for more sustainable hydrophobic coatings

Valentina Dichiarante,[†] Maria I. Martinez Espinoza,[†] Lara Gazzera,[†] Maja Vuckovac,[‖] Mika Latikka,[‖] Gabriella Cavallo,[†]* Giuseppina Raffaini,[†] Reinier Oropesa-Nuñez,[‡] Claudio Canale,[§,‡] Silvia Dante,[‡] Sergio Marras,[‡] Riccardo Carzino,[‡] Mirko Prato,[‡] Robin H. A. Ras,[‖,#] and Pierangelo Metrangolo[†,‖]*

[†] Department of Chemistry, Materials and Chemical Engineering "Giulio Natta", Politecnico di Milano, Via L. Mancinelli 7, 20131 Milan, Italy
[‖] Department of Applied Physics, Aalto University School of Science, Puumiehenkuja 2, 02150 Espoo, Filand
[‡] Nanophysics Department, Istituto Italiano di Tecnologia, 16163, Genova, Italy
[§] Department of Physics, University of Genova, 16146, Genova, Italy
[#] Department of Bioproducts and Biosystems, Aalto University School of Chemical Engineering, Kemistintie1, 02150 Espoo, Finland

ABSTRACT: Perfluorocarbons (PFCs) have proven to be very efficient in building up omniphobic surfaces because of the peculiar properties of fluorine atoms. However, due to their environmental impact and bioaccumulative potential, perfluorinated surfactants with chains longer than six carbon atoms have been banned, and other alternatives had to be found. Herein, we demonstrate the possibility to build omniphobic self-assembled monolayers (SAMs) using a multibranched fluorinated thiol (BRFT) bearing ultrashort fluorinated alkyl groups, surrounding a hydrocarbon polar core. This unique design allows us to multiply the number of fluorine atoms in the molecule (27 F atoms per molecule), affording a high fluorine density on the surface and a low surface free energy. Moreover, the presence of four ether bonds in the core may hasten molecular degradation in the environment because of the cleavage of such bonds in physiological conditions, thus overcoming bioaccumulation issues. BRFT may effectively represent a valuable substitute of long-chain perfluoroalkyl thiols. In fact, BRFT SAMs show the same hydrophobic and oleophobic performances of standard linear perfluoroalkyl thiols (such as 1H,1H,2H,2H-perfluorodecanethiol, PFDT), giving rise to more stable surfaces with a better frictional behavior. Superhydrophobicity was also observed with SAMs grown on nanostructured Cu/Ag surfaces. Our results have proven the ability of short-chain multibranched fluorous molecules to behave as suitable replacements for long-chain perfluoroalkanes in the field of surface coatings. Our molecules may be applied to various surfaces because of the available multiple choice of linker chemistry.

KEYWORDS: Perfluorocarbons, Self-assembled monolayer, Gold, Superhydrophobic surfaces, Thiol

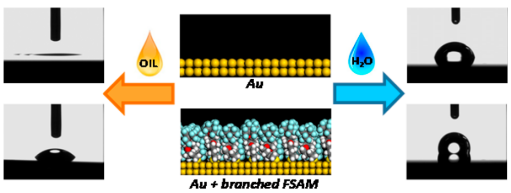

INTRODUCTION

Nonwetting coatings represent a key target for current materials science due to their potential applications in self-cleaning, anti-icing, antifouling, antiadhesive, and corrosion-resistant surfaces. Many research efforts focused on the development of either superhydrophobic or superoleophobic surfaces, i.e., showing, respectively, water or oil contact angles >150°, or even more advantageous "omniphobic" surfaces being water- and oil-repellent at the same time.[1,2] Taking inspiration from nature, the best results were obtained combining micro- and nanoscale hierarchical structures with low-surface-energy materials, such as fluorinated polymers, silanes, thiols, surfactants, and plasma.[3]

Self-assembled monolayers (SAMs) of either organosilanes or thiols played a major role in the achievement of new functional surface properties.[4] The self-assembly process reproducibly generates highly ordered and robust films, less prone to wear than polymeric modifiers.[5] Fluorinated SAMs (FSAMs) derived from the adsorption of long-chain perfluorinated organic thiols on gold, proved to be particularly efficient in building up superhydrophobic and superoleophobic surfaces, since the introduction of a fluorocarbon segment changes important physical properties of the resulting films,

Received: February 16, 2018
Revised: June 18, 2018
Published: July 16, 2018

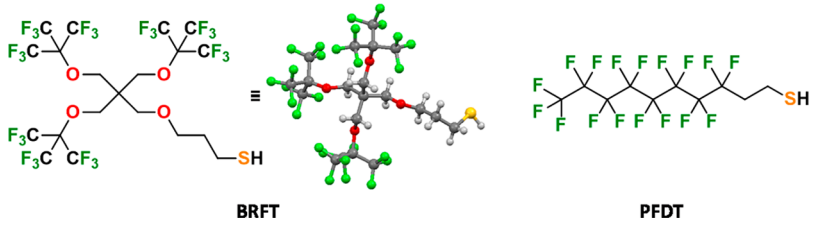

Figure 1. Chemical structure of branched highly fluorinated thiol used in the present work (BRFT) and of linear 1H,1H,2H,2H-perfluorodecanethiol (PFDT).

including friction and wettability.[6] Unfortunately, linear-chain perfluorocarbons (PFCs) with more than six CF_2 units show long-lasting persistence in the environment, high tendency to accumulate in humans and animals, and suspected toxicity.[7] For these reasons, they were recently banned and thus need to be replaced by more sustainable alternatives.[8] The search for less harmful but similar performing coating agents focused mainly on shorter PFC chains ($\leq C_4$), whose lower lipophilicity reduces bioaccumulation.[9] Recently, for example, superhydrophobic silica coatings were prepared by a sol−gel process using a fluorinated polymeric sol−gel precursor synthesized by copolymerization of 2,3,4,5,5,5-hexafluoro-2,4-bis-(trifluoromethyl)-pentyl methacrylate with a nonfluorinated silane, instead of long-chain perfluoroalkyl silanes.[10] Obviously, simply cutting down the chain length does not lead to satisfactory results in balancing environmental impact and performance. Indeed, short fluorinated chains undergo surface rearrangements after prolonged contact with water or other liquids since their lower self-organization behavior induces high mobility at the external surface.[11]

An interesting approach to obtain either superhydrophobic or superoleophobic surfaces was offered by electropolymerization of fluorinated pyrenes and 3,4-ethylenedioxypyrroles (EDOP), respectively.[12,13] The appropriate tuning of both the fluorinated chain length and the alkyl spacer allowed for improving their oil-repellent behavior.[14−16] If F-butyl, F-hexyl, and F-octyl 3,4-ethylenedioxythiophenes (EDOT) with an amide connector were used as monomers, superhydrophobic properties were achieved, independently of the fluorinated chain length, whereas only F-butyl tails afforded superoleophobic surfaces ($\theta_{\text{sunflower oil}}$ = 150° and $\theta_{\text{hexadecane}}$ = 132°).[17] Furthermore, superomniphobic coatings on fabrics, paper, and sponges obtained from fluorinated copolymers with short perfluorobutyl side chains were reported by Jiang et al.[18] They also demonstrated that a suitable choice of spacer group and crystalline hydrocarbon component limit surface molecular motion and promote dynamic water repellency. Electropolymerization of 3,4-propylenedioxythiophene monomers containing a branched PFC chain produced superhydrophobic films similar to those of linear PFC chains with the same number of C−F bonds. Interestingly, the branching induced a much higher oil repellency.[19]

Multibranched highly fluorinated compounds bearing perfluoro-*t*-butoxy groups actually combine the advantages of a high number of fluorine atoms, short fluorinated chains, and enhanced lability and biodegradability of ethereal groups.[20] A thiol incorporating such a multiarm fluorous scaffold (BRFT, Figure 1) was recently applied to the stabilization of gold nanoclusters.[21]

Herein, we demonstrate that the same thiol forms efficient omniphobic SAMs on gold substrates with a more satisfactory frictional response than that obtained with linear 1H,1H,2H,2H-perfluorodecanethiol (PFDT) and also affords superhydrophobic coatings on properly rough starting surfaces.

The overall innovation potential of our coating agent is high because of its easy scalability and great versatility. In fact, its molecular structure can be easily modified to replace the thiol moiety with different anchoring groups, e.g., $-CO_2H$, OH, NH_2, etc., opening a plethora of applications on various surfaces.

MATERIALS AND METHODS

Commercially available silver nitrate (99% Fluka), PFDT (97% Aldrich), dichloromethane (DCM, 99% Aldrich), and ethanol (96% Carlo Erba) were used as received. BRFT thiol was synthesized according to a previously reported procedure.[21] Gold (Au) chips obtained from PoliFAB were prepared by e-beam evaporation of a gold layer of about 30 nm thickness on a silicon wafer covered with a titanium layer of about 10 nm. Prior to use, Au chips were washed with deionized water, dried under air flux, and treated by a UV ozone cleaner for 30 min. SAMs were obtained by dipping the chips in a 1 mM ethanol solution of the thiol for 24 h, then rinsing with clean ethanol and drying under nitrogen flux. Blank chips were prepared following the same cleaning and rinsing procedure, except for the dipping step, and used as reference. The copper (Cu) samples were prepared from a commercially available 1 mm thick copper sheet (99.8% purity) by cutting into plates with 3 cm × 5 cm dimensions. Then, the copper plates were mechanically polished with sandpaper and washed with Milli-Q water and acetone to eliminate the surface contamination. Fluorinated nanostructured Cu/Ag surfaces were prepared following the method described in the literature.[22] Copper substrates were cleaned and polished to create microscopic surface roughness; then, they were coated with silver by immersing them in 10 mM aqueous $AgNO_3$ solution for 60 s, followed by washing with Milli-Q water and drying under nitrogen flow. Subsequently, substrates were immersed in 1 mM PFDT or BRFT solution in DCM for 10, 30, 120, or 240 min. After chemical surface modification, substrates were washed twice with fresh DCM and dried in ambient conditions.

Thiol-functionalized surfaces were characterized by measuring static and dynamic contact angles (CAs), as well as sliding angles of deionized water and model oily compounds (e.g., *n*-dodecane, mineral oil). Static CAs were measured using the sessile drop method (4 μL drop volume, five different spots for each chip). For each chip, measurements were performed immediately after functionalization and then repeated after 7 and 14 days. Advancing contact angles were measured by placing a 1 μL droplet on the surface and increasing its volume to 20 μL, at a rate of 0.05 μL/s. Receding contact angles were measured by decreasing the droplet volume at a rate of 0.05 μL/s, starting from a droplet volume of 20 μL. Sliding angles for Au chips were determined for water and mineral oil, using the tilting plate method, varying the stage inclination angle at 1 deg/s Surface free energies were estimated by means of the Owens−Wendt−Rabel−Kaelble (OWRK) method, using water, glycerol, DMF, and DMSO as contacting liquids.[23,24] Morphology of bare Au substrate and fluorinated monolayers was analyzed by atomic force microscopy (AFM). Frictional behavior of Au substrates was evaluated both in air and in water by means of lateral force microscopy (LFM)

measurements. For Cu/Ag surfaces, the friction coefficient was determined using droplet oscillations, measuring 3−4 different spots on each sample and 9−12 oscillations per sample.[25]

X-ray photoelectron spectroscopy (XPS) was used to analyze the chemical composition of the surfaces and provide evidence of thiol binding to the gold surface. Thickness and roughness of the monolayers and scattering length density (SLD) profiles were determined by X-ray reflectivity. Molecular dynamics (MD) studies were performed according to a previously reported simulation protocol.[26] Very good agreement was found between experimental data and theoretical results about the wettability of the fluorinated surfaces and also about the thickness of the two films. A detailed description of all experimental conditions and instruments used can be found in the Supporting Information.

RESULTS AND DISCUSSION

Molecular Modeling. In order to predict molecular conformations and mobility of fluorinated alkanethiol chains covalently attached on gold surfaces, we performed preliminary investigations using MD simulations. In particular, we compared a FSAM made by PFDT with the one made by our branched thiol (BRFT). FSAM/water interfaces were also modeled to study their interactions with water. In our simulations, we assumed a perfect crystalline packing of gold substrates with perfectly flat and uniform surfaces. Figure 2 reports a molecular dynamics visualization of FSAMs and FSAM/water interfaces after a 2 ns simulation time.

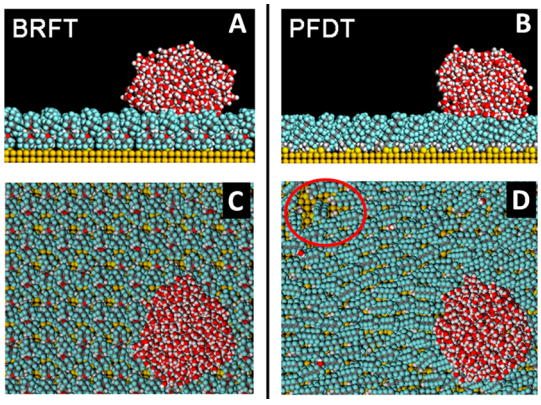

Figure 2. Molecular dynamics visualization of FSAMs and FSAM/water interfaces in spacefilling models: (A) lateral and (C) top views of BRFT SAM and (B) lateral and (D) top views of PFDT SAM after 2 ns of simulation time.

Changes in molecular conformations have been investigated by calculating the maps of the root-mean-square distance (RMSD) and measuring the distances between corresponding atoms in the dynamic trajectories. This allowed us to recognize families of closely related conformers (Figure S1a). Our analysis revealed larger conformational changes in PFDT chains than in BRFT. Moreover, some linear chains in PFDT SAM can even bend through a *gauche* conformation around a single C−C bond, leading part of the chain to adopt an arrangement almost parallel to the surface. Such bending appears to be cooperative among neighboring chains, producing a local parallel ordering of fluorinated chains and exposing some gold "islands" clearly visible in the upper left corner of Figure 2D. On the other hand, we observed a higher positional ordering in BRFT SAM, where the only possible rearrangement involves a free rotation around the O−C$(CF_3)_3$ bond in the fluorinated "umbrella" exposed on the surface (Figure S1b). These conformational changes, however, do not affect the overall morphology of the flat BRFT surface. Therefore, our study demonstrated a larger conformational freedom for the linear thiol with respect to the branched one, whose mobility becomes further restricted in the presence of a water drop, as shown by RMSD maps in Figure S1a. This suggests a tighter molecular packing and a higher rigidity of the BRFT SAM.

In order to better describe the local disorder in the PFDT film with respect to the well-ordered BRFT film, we also studied the distance of the carbon atoms that are topologically *farthest* from the surface for the two different films (Figure S2a) and the pair distribution function (PDF) of fluorine atoms from the gold surface (Figure S2b). The simulation results suggest a layer thickness of about 12.7 Å in the case of PFDT and of 10.1 Å in BRFT. Furthermore, the PDF allowed us to get information about the packing density of fluorinated thiols on gold surface. In the simulation cell, the number of chains covalently bound to gold atoms is 196 and 98 for PFDT and BRFT SAMs, respectively (see SI for details). This is fully consistent with the different steric hindrance of the two thiols. In fact the van der Waals volume calculated for the branched thiol is almost twice the volume calculated for PFDT (258 $Å^3$ for PFDT and 497 $Å^3$ for BRFT). The same trend is also found for the exposed surface areas (312 $Å^2$ for PFDT and 570 $Å^2$ for BRFT). Such data suggest a 20% larger density of fluorine atoms for PFDT compared to BRFT film.

Finally, in order to study FSAM/water interfaces, we modeled a water drop in contact with both fluorinated surfaces. At the end of the dynamical simulation, the drop kept a roughly spherical shape suggesting large contact angles, as would be expected for fluorinated surfaces (see Figure S3 and the four animations of the MD runs in the SI). Interestingly, PDF allowed us to study the distribution of water molecules on the fluorinated films, mapping hydrogen and oxygen atoms for both water molecules and water droplets as a function of their distance from gold (Figure S3b). For PFDT SAM, we found a minimum H−Au distance of 9 Å, which is a bit lower than the thickness of the layer. This is because very few water molecules can somewhat penetrate in the upper part of the deposited film (Figure S3b, right). On the contrary, for BRFT film, the MD run reveals that water molecules never penetrate inside this ordered hydrophobic film (Figure S2b). Moreover, the PDF of the water molecules on the BRFT SAM is more symmetric, indicating a more spherical shape of the water drop in contact with this fluorinated film, as already pointed out from the analysis of the RDF of water molecules (Figure S3a).

X-ray Photoelectron Spectroscopy (XPS). XPS measurements were performed on three different samples, namely, a bare Au substrate and Au substrates coated with PFDT and BRFT SAMs. Before the analysis, the bare Au substrate was cleaned in a vacuum chamber by Ar^+ ions sputtering (ions energy: 4 keV; sputtering time 30 s), in order to remove all possible environmental contaminations and provide a reliable reference for a clean gold surface. Figure 3 reports high resolution scans of the F 1s, S 2p, and Au 4f regions of the spectra collected on the three samples. As expected, the gold substrate after Ar^+ sputtering shows only peaks related to the presence of Au, while PFDT and BRFT SAMs are characterized by the presence of signal due to F, C, O, and S.

F 1s spectra for both PFDT and BRFT SAMs are characterized by a single peak centered at 688.1 ± 0.2 and 688.6 ± 0.2 eV, respectively. This position is in agreement with

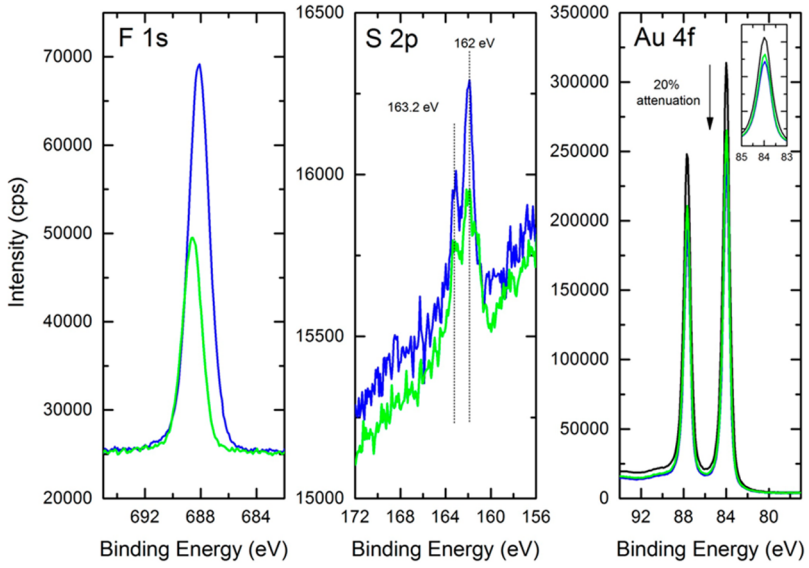

Figure 3. XPS spectra of bare Au substrate (black curve) and Au substrates coated with PFDT SAM (blue curves) and BRFT SAM (green curves): F 1s (left), S 2p (middle), Au 4f (right).

literature reports about fluorinated organic compounds and is indicative of $-CF_2$ and $-CF_3$ moieties.[27]

Concerning the sulfur binding energy region, both samples are characterized by an S 2p doublet having the main component centered at 162.0 ± 0.2 eV. The observed position is consistent with literature data and is assigned to the formation of a thiolate S−Au bond between the thiol group and Au substrate.[28] In the case of the BRFT film, a shoulder in the S 2p signal appears at 161.2 ± 0.2 eV, which can be attributed to X-ray damage.[29]

The Au 4f signals collected on PFDT and BRFT films show a reduced intensity with respect to those collected on a clean Au substrate. This attenuation—in the order of roughly 20% for both films—is the typical signature of the presence of a film on top of a substrate.[30] From the ratio between the Au 4f peak area of fluorinated SAMs and bare Au substrate, we were able to calculate a film thickness of 9 ± 2 Å for BRFT SAM and 12 ± 2 Å for PFDT SAM which are in good agreement with computational data. Finally, the packing density of fluorinated SAMs can be correlated to the Au 4f/F 1s peak area ratios, after normalization to the corresponding relative sensitivity factors (RSF, a parameter that can be related to the cross section of the X-ray induced photoemission process). We calculated Au/F ratios of 1.03 and 2.18, respectively, for PFDT and BRFT SAMs. This would suggest a higher number of fluorinated molecules per unit area in PFDT SAM than in BRFT SAM. These data perfectly agree with computational analysis and can be easily explained taking into account the different steric hindrance of the two molecules.

X-ray Reflectivity Analysis. Fluorinated monolayers on flat gold surfaces were characterized through X-ray reflectivity (XRR) analysis in order to measure, besides thickness and roughness, also the scattering length density (SLD), a parameter that can be directly correlated to fluorine density. The reflectivity curves obtained from bare Au substrates and Au substrates coated with PFDT and BRFT SAMs are reported in Figure S4. The interference pattern measured on the starting Au substrate was quite complex since it is composed of several different layers ($Si/SiO_2/Ti/Au$) of known thickness *d*. Anyway, it was possible to measure X-ray reflectivity of both thiol films and to calculate their thickness and roughness taking into account the background response given by the bare Au substrate themselves. The reflectivity R from both the thiol-coated surfaces differs significantly from that reflected from bare Au substrate, and a small, yet significant, difference between PFDT and BRFT SAMs reflectivity was observed. The curves were fitted with slab models of uniform SLD, thickness *d*, and roughness σ, taking into account the layered structure of the substrate and the chemical composition of the fluorinated SAMs. SAMs were modeled with a single slab, and the best curve fits were obtained considering also Au thickness as a free parameter. Table 1 summarizes the parameters of the best-fit curves reported in Figure 4. We found an average roughness of 7.8 ± 0.5 Å for both SAMs and a similar layer thickness of about 10 Å (9.4 ± 0.9 and 10.6 ± 0.8 Å for PFDT and BRFT, respectively), as confirmed by XPS measurements. These last values are in good agreement with molecular dimensions of the branched thiol measured from its X-ray single crystal structure[21] and further prove that BRFT actually forms a

Table 1. Values of Thickness, Roughness, and Scattering Length Density (SLD) obtained by XRR Measurements for Branched and Linear Fluorinated Films on Gold Chips[a]

	d (Å)	SLD (10^{-6} Å^{-2})	σ (Å)
PFDT	9.4 ± 0.9	8.0 ± 0.5	7.0 ± 0.8
Au	280.6 ± 0.7	122.5 ± 0.5	7.4 ± 0.5
Ti	*100.5 ± 0.7*	*36.5*	*7.5 ± 0.6*
SiO_2	*20.3 ± 0.5*	*18.9*	*3.2 ± 0.5*
Si (bulk)		*20.1*	*3.1 ± 0.5*
BRFT	10.6 ± 0.8	14.3 ± 0.5	7.1 ± 0.7
Au	277.6 ± 0.5	121.5 ± 0.6	7.4 ± 0.6
Ti	*100.5 ± 0.7*	*36.5*	*7.5 ± 0.6*
SiO_2	*20.3 ± 0.5*	*18.9*	*3.2 ± 0.6*
Si (bulk)		*20.1*	*3.1 ± 0.5*

[a]Background values of uncoated Au substrates are also reported. Values in italics are kept fixed when fitting SAM reflectivities.

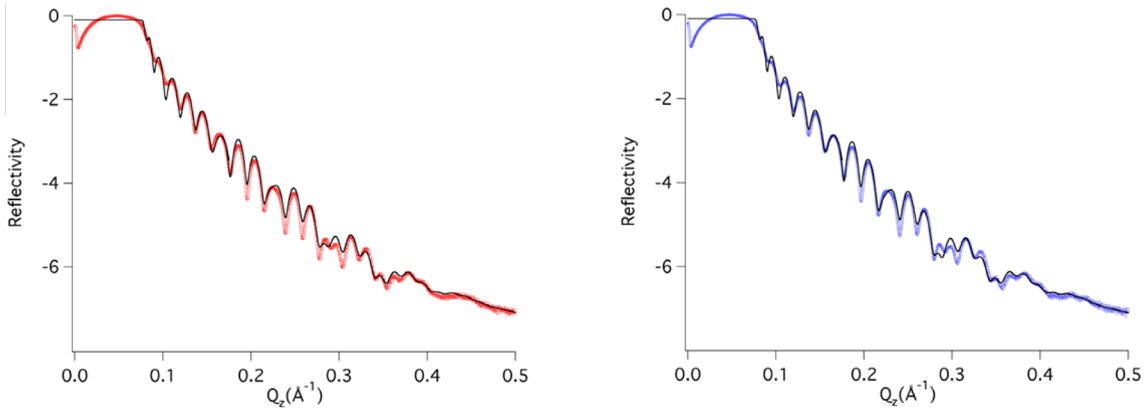

Figure 4. XRR curves of Au chips, coated with (A) PFDT SAM (red curve) and (B) BRFT SAM (blue curve) and their respective best fit curves (black curves).

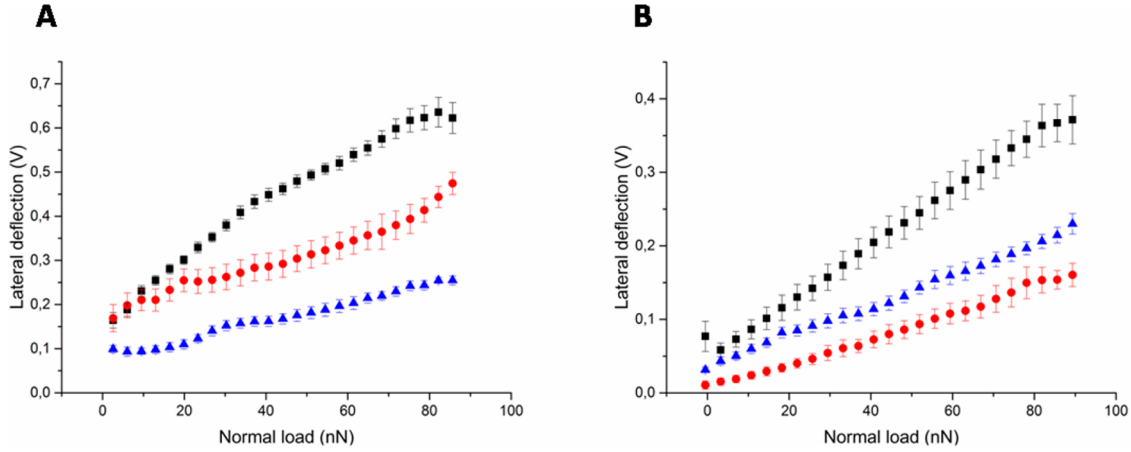

Figure 5. Frictional behavior of bare Au chip (black square), PFDT (red circle), and BRFT (blue triangle) SAMs studied by lateral force microscopy (LFM) in air (A) and water (B).

monolayer on Au surfaces. SLD values are in good agreement with electron density reported for perfluorinated alkyl thiols, with a slightly higher electron density for BRFT, suggesting a higher fluorine density for BRFT SAMs.

Frictional Behavior of Functionalized Au Surfaces. Atomic force microscopy (AFM) was used to assess the morphology of fluorinated gold surfaces. AFM measurements gave an average roughness of 7 ± 1 Å for PFDT and 8 ± 1 Å for BRFT (Figure S5), confirming XRR data. Both roughness and morphology of the fluorinated surfaces are very similar to the bare Au substrate, 7 ± 1 Å (Figure S5), as would be expected in the presence of a homogeneous thin film. Interesting results were obtained measuring through lateral force microscopy (LFM) the lateral deflection signal while the AFM cantilever scans the surface in imaging mode. LFM allows us to study the frictional behavior at nanometer scale since the lateral deflection signal, generated by the cantilever torsion, is proportional to the friction between the silicon AFM probe and the surface. These experiments were performed both in air and in water. In air, as shown in Figure 5A, the presence of a fluorinated layer reduces the friction compared to bare gold; however, BRFT produces a much more pronounced effect than that exerted by PFDT. These findings, correlated with the morphological analysis, indicate that PFDT and BRFT do form homogeneous layers on the gold surface. Moreover, these results would suggest that fluorinated SAMs made by the branched thiol are more rigid and tightly packed than the ones made by linear chains. In fact, besides the chemical nature, the frictional behavior of SAM is also affected by the packing and thickness of the monolayer. It is well known that in amorphous monolayers the presence of defects and structural disorder contributes to energy dissipation through the activation of rotational and vibrational modes in the molecules, producing higher friction.[30] On the contrary, films with well-ordered structures show lower friction coefficients than similar but more disordered films. Therefore, a higher monolayer rigidity results in a much better lubrication effect.[31] Generally, monolayers made by short-chain perfluorocarbons show friction coefficients higher than long-chain perfluorocarbons because of their poor packing. Here, the trend is reversed, probably because of the branched structure of our thiol that plays an essential role in stabilizing the monolayer and promoting a tight molecular packing. Our hypothesis can be further supported by the higher crystallinity of bulk BRFT with respect to PDFT. Indeed, at room temperature, PFDT is a liquid, whereas BRFT is a crystalline solid because of the presence of multiple F···F interactions among CF_3 groups of adjacent molecules in the crystal structure.[21] We may speculate that the same interactions are also occurring in the monolayer and can be responsible for the higher rigidity and order of BRFT SAM.

Another key point is the different frictional behaviors observed in water (Figure 5B). While BRFT performed as in air, PFDT gave much lower deflection values than in air, and

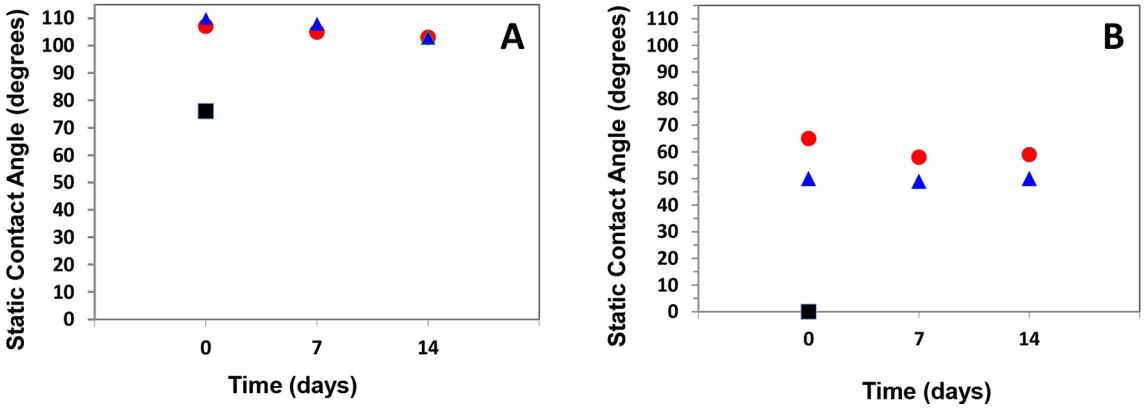

Figure 6. Time evolution of static contact angle on PFDT SAM (red circle) and BRFT SAM (blue triangle) measured with (A) water and (B) *n*-dodecane. CAs measured on bare Au substrate (black square) are also reported as reference. CA measurements were done immediately after SAM preparation, and then substrates were dried with nitrogen and stored under ambient laboratory conditions before repeating measurements after 7 and 14 days. Each value is the average of five measurements on each sample.

Table 2. Static (θ_{Stat}), Advancing (θ_{Adv}), and Receding (θ_{Rec}) Contact Angles, Contact Angle Hysteresis ($\theta_{Adv} - \theta_{Rec}$), and Sliding Angles Measured with Different Liquids for PFDT and BRFT SAMs on Gold Surfaces

	Water					Oil		Glycerol	DMF	DMSO
	θ_{stat} [a]	θ_{Adv}	θ_{Rec}	(θ_{Adv}-θ_{Rec})	θ_{slid}	θ_{stat} [a]	θ_{slid} [b]	θ_{stat}	θ_{stat}	θ_{stat}
PFDT	107 ± 3	115	108	7	30	65 ± 2	35	106 ± 1	80 ± 1	86 ± 1
BRFT	110 ± 1	113	107	6	35	50 ± 2	25	102 ± 1	78 ± 1	83 ± 1

[a]Contact angles are mean values based on five measurements. Oil static CA (θ_{stat}) has been measured using *n*-dodecane as the model for oil and apolar liquids. [b]Measured using mineral oil.

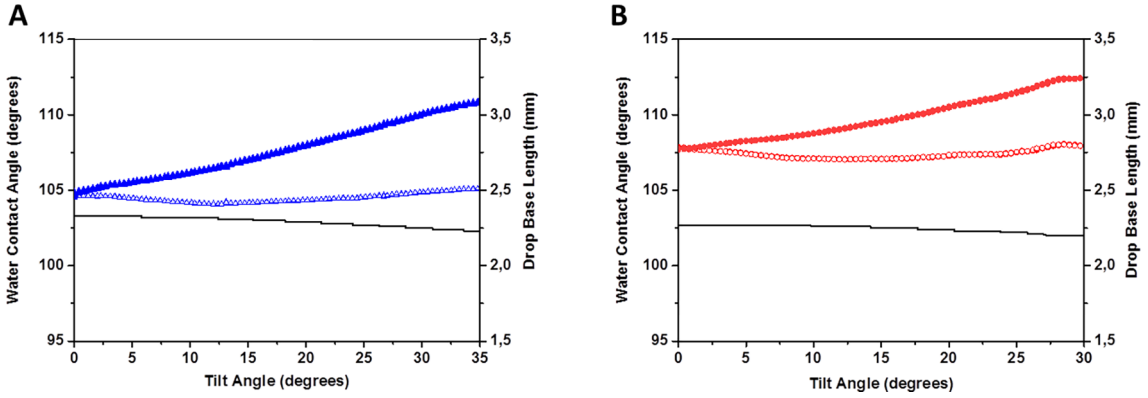

Figure 7. Maximum (θ_{max}, filled symbols) and minimum (θ_{min}, empty symbols) water contact angles for advancing and receding fronts and drop base length of water (black line), measured at different tilting angles on Au chips functionalized with (A) BRFT and (B) PFDT. Each measurement point has a 0.1° error bar.

even lower than those of the branched thiol. This behavior would suggest that PFDT monolayers underwent some kind of surface reconstruction in the presence of water,[32] i.e., linear perfluoralkyl chains tend to bend and rearrange to minimize contact with water, whereas the more rigid and crystalline film made by BRFT does not change its packing mode and chain alignment. Therefore, BRFT seems to determine a higher structural stability of the monolayer, which is less affected by changes in environmental conditions, i.e., humidity changes.

Wettability of Fluorinated Gold Surfaces. Surface wettability was studied by static contact angle (CA) measurements using deionized water and *n*-dodecane as contacting liquids. When water was dropped on gold surfaces, bare Au led to a CA of 76° ± 5°, while in the presence of thiols CA values of 107° ± 3° and 110° ± 1° for PFDT and BRFT, respectively, were measured (Figure 6A), which are in good agreement both with theoretical calculations and with literature data.[33] Measuring CAs with *n*-dodecane as the model for oil and apolar liquids, again we found that both thiols are able to reduce the wettability of the starting Au surface. While *n*-dodecane droplets on bare Au tend to spread flat, making any measurement impossible, CAs of 50° ± 2° and 65° ± 2° have been measured for BRFT and PFDT, respectively (Figure 6B). Both the increase in hydrophobicity and the decrease in oleophilicity are consistent with the presence of SAMs on gold surfaces. There are no marked differences between the two thiols, except that the linear thiol seems to be slightly more oleophobic than the branched one. In order to probe the stability of fluorinated SAMs, both PFDT- and BRFT-coated substrates were left to equilibrate under ambient laboratory

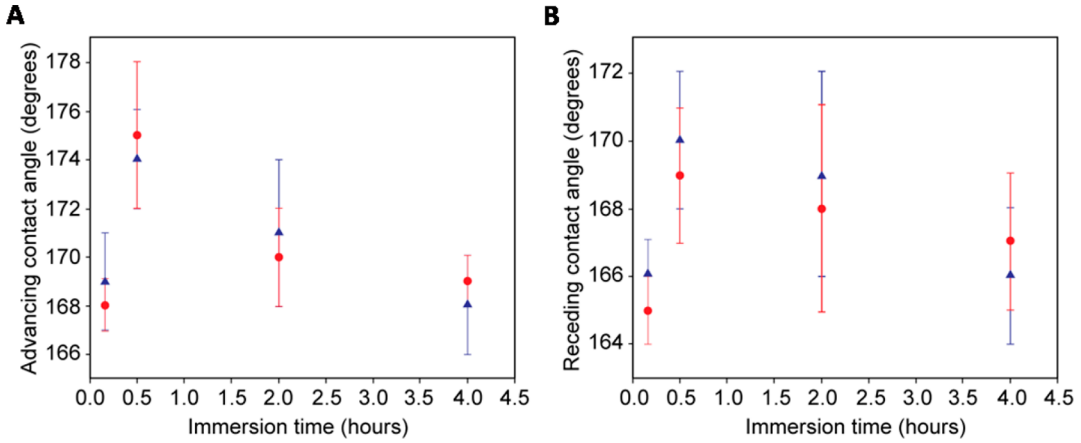

Figure 8. (A) Advancing and (B) receding water contact angles measured at different deposition times on Cu/Ag substrates functionalized with PFDT (red circle) and BRFT (blue triangle). Each value is the average of 15 different spots measured on each sample, while error bars denotes standard deviation.

conditions for a few weeks, and static CA measurements were repeated after 7 and 14 days. Both water and oil CA values were only slightly decreasing with time, demonstrating the high stability of fluorinated SAMs.

Advancing (θ_{Adv}) and receding (θ_{Rec}) water CAs for PFDT and BRFT SAMs on Au surfaces were measured also with the sessile drop method. Results are reported in Table 2 along with the respective contact angle hysteresis (CAH = $\theta_{Adv} - \theta_{Rec}$). Water CA values are quite similar for both SAMs, and contact angle hysteresis is quite small, indicating that both surfaces are smooth and homogeneous.

Using the tilting plate method, we monitored the sliding behavior of both water and mineral oil droplets on fluorinated SAMs (Figure 7 and Figure S6). Here, 4 μL droplets were displaced on the tested substrate, and the evolution of the contact angles at the lowest point (advancing front) and at the highest point (receding front) of the contact line was measured while the substrate was tilted from the horizontal position. Because of the platform tilting, the droplet deformed its shape as an effect of gravity and adhesion forces acting on it. After a certain tilting angle, gravity becomes more important than the adhesion force, and the droplet started to move as well as the contact line (droplet diameter increases here). The angles at which the contact line shifts are named maximum (θ_{max}) and minimum (θ_{min}) contact angles for the advancing and receding fronts, respectively. In Figure 7A and B, it can be seen that on tilting the platform the base diameter of water droplets remained almost constant with both thiols, whereas θ_{max} increased at a faster rate compared to the corresponding decrease in θ_{min}. At higher surface tilting, droplets began to slide down while reaching the respective sliding angle, 30° for PFDT and 35° for BRFT. At this point the values of θ_{max} and θ_{min} are 113° and 107° for PFDT, respectively, and 111° and 105° for BRFT, respectively, almost equivalent to the advancing and receding CAs measured with the sessile drop method. Although it is still under debate,[34] in the present study, both methods gave an accurate evaluation of the CAH.

When mineral oil was used as the contacting liquid, a completely reversed behavior was observed: The decrease in θ_{min} was much faster than the corresponding increase in θ_{max}, and the drop base diameter grew with tilting (Figure S6). The oil sliding angle on PFDT SAM was 35°, similar to the one found for water, while for the branched thiol the sliding angle was quite smaller being only 25°.

Typically, low CA hysteresis and sliding angles <10° are required to ensure liquid droplets roll away easily without contaminating the surface.[35,36] Having higher sliding angles, our fluorinated gold surfaces cannot be termed as "self-cleaning", although their low resistance to sliding confirmed the hydrophobic and oleophobic properties already shown by static CA measurements.

In order to probe the influence of surface dipoles on surface wettability,[37] in addition to water and nonpolar solvents (oil and dodecane), we also measured the static contact angles with liquids of different polarity. In particular, we chose glycerol as the polar protic liquid and DMF and DMSO as the polar aprotic liquids. Results are reported in Table 2. Changing both polarity and proticity of the contacting liquids did not produce any marked difference between the two thiols. This allows us to exclude any particular influence of surface dipoles on the observed coating wettabilities.

Surface free energy values were also determined by the OWRK method,[23,24] using water, glycerol, DMF, and DMSO as contacting liquids. We found very similar and quite low values for both fluorinated monolayers. In fact, the surface free energies are 12.7 ± 0.4 and 13.7 ± 0.6 mJ/m^2 for PFDT and BRFT, respectively, in good agreement with literature data for fluorinated SAMs.[38,39] These values are quite small if compared to poly(tetrafluoroethylene) coatings (22 mJ/m^2)[40] and can be explained supposing an uniform hexagonal closed alignment of $-CF_3$ groups over the surface.[41]

Superhydrophobic Surfaces. It is well known that the wetting behavior of a surface results from the appropriate combination of surface chemistry and morphology. Generally, increasing the roughness of a hydrophobic surface causes higher CA values, and superhydrophobicity can be obtained.[33] With this in mind, we decided to study the wetting behavior of PFDT and BRFT SAMs grown on nanostructured Cu/Ag surfaces, prepared according to ref 22. Scanning electron microscopy (SEM) images of the obtained silver-coated substrates are reported in Figure S7. Static water CA of such a nanostructured surface has been measured to be 120° ± 2°. Fluorinated monolayers were prepared by treating Cu/Ag nanostructured surfaces with PFDT or BRFT solutions for four different immersion times (10, 30, 120, and 240 min).

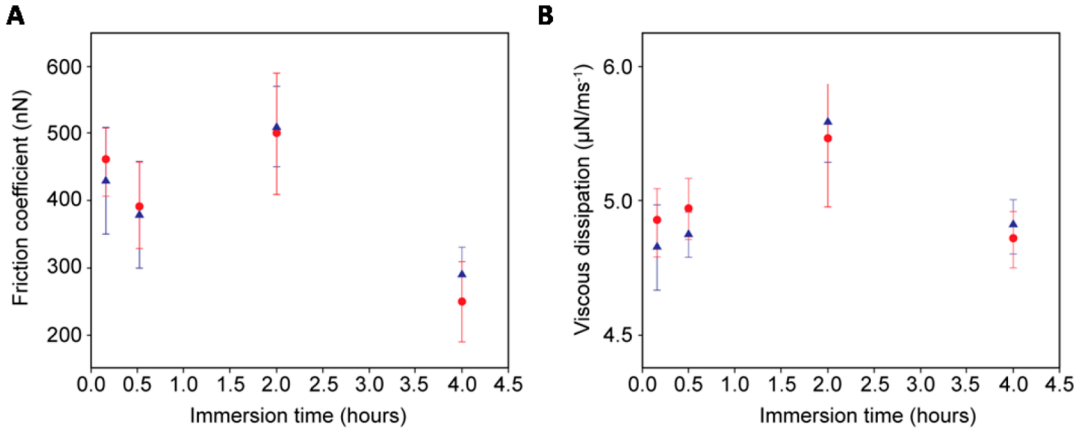

Figure 9. (A) Average friction coefficients and (B) viscous dissipation parameters measured as a function of immersion time for Cu/Ag substrates functionalized with PFDT (red circle) and BRFT (blue triangle). Each value is the average of 10 measurements on each sample, while error bar denotes standard deviation.

Advancing and receding contact angles were measured on 15 different spots per sample and are plotted as a function of immersion time in Figure 8. As expected, by introducing roughness, surface contact angles are considerably increased, and superhydrophobicity is provided (Figure 8). As in the case of flat gold substrates, again, we did not find any marked difference between the two thiols. It is worth noting here that despite the short immersion time for both thiols it was possible to obtain a homogeneous monolayer already after 10 min, demonstrating the high efficiency of the self-assembly process.

For studying magnetically induced droplet motion on superhydrophobic surfaces, aqueous ferrofluid was prepared as reported in the Supporting Information. Energy dissipation parameters, friction coefficients, and viscous dissipations for the above-mentioned samples were obtained by performing oscillations 10 times for each sample. Obtained F_{CAH} and β are plotted as a function of deposition times (Figure 8). On the basis of dynamic contact angles (Figure 8) and energy dissipation parameters (Figure 9), there was no significant difference between the two thiols.

CONCLUSIONS

In summary, we have reported a new fluorinated coating agent characterized by a multibranched structure with short fluorinated alkyl groups surrounding a hydrocarbon polar core able to self-assemble on surfaces, forming omniphobic monolayers. On smooth gold substrates, we demonstrated that its coatings give the same hydrophobic and oleophobic performances of standard linear perfluoroalkyl thiols (such as PFDT). Interestingly, we found a better frictional behavior of BRFT respect to PFDT. This suggests a higher ability of BRFT to form well-ordered, stable, and robust monolayers whose rigid and tightly packed structure is responsible for their high stability, in agreement with the theoretical study. A similar behavior was also demonstrated on nanostructured surfaces, which yielded superhydrophobic coatings.

BRFT may effectively represent a valuable substitute of long-chain linear perfluoroalkyl thiols. The peculiar structure of BRFT affords a high fluorine content, and it is expected a higher biocompatibility of the materials, lessening bioaccumulation and bioconcentration concerns. In fact, the presence of four ether bonds in the core may hasten molecule degradation in the environment because of the cleavage of such bonds in physiological conditions, thus overcoming bioaccumulation issues and leading to high cellular compatibility. Biocompatibility and biodegradability of BRFT are currently under investigation and will be reported elsewhere.

ASSOCIATED CONTENT

Supporting Information

The Supporting Information is available free of charge on the ACS Publications website at DOI: 10.1021/acssuschemeng.8b00777.

Synthetic methods, molecular dynamics simulations, X-ray reflectivity (XRR) measurements, X-ray photoelectron spectroscopy (XPS), atomic force microscopy (AFM) measurements, lateral force microscopy (LFM) measurements, contact angle and surface free energy measurements, ferrofluid synthesis, and harmonic magnetic droplet oscillations. (PDF)

Animation of MD run in the presence of water drop for PFDT and BRFT:

MD simulation (Au−BRFT−water, 2 ns, side). (AVI)

MD simulation (Au−BRFT−water, 2 ns, top). (AVI)

MD simulation (Au−PFDT−water, 2 ns, side). (AVI)

MD simulation (Au−PFDT−water, 2 ns, top). (AVI)

AUTHOR INFORMATION

Corresponding Authors

*Gabriella Cavallo: E-mail: gabriella.cavallo@polimi.it. Tel.: 0039 02 2399 3046. Fax: 0039 02 2399 3080.

*Valentina Dichiarante: E-mail: valentina.dichiarante@polimi.it. Tel.: 0039 02 2399 3159. Fax: 0039 02 2399 3080.

ORCID

Valentina Dichiarante: 0000-0002-2977-5833

Maja Vuckovac: 0000-0001-5895-7612

Reinier Oropesa-Nuñez: 0000-0002-9551-6565

Silvia Dante: 0000-0001-6906-8482

Mirko Prato: 0000-0002-2188-8059

Robin H. A. Ras: 0000-0002-2076-242X

Pierangelo Metrangolo: 0000-0002-7945-099X

Author Contributions

The manuscript was written through contributions of all authors. All authors have given approval to the final version of the manuscript.

Funding

The European Research Council (ERC) is acknowledged for granting the project 307108. Fondazione Cariplo, project 2014−0746 is also acknowledged.

Notes

The authors declare no competing financial interest.

ABBREVIATIONS

PFDT, 1H,1H,2H,2H-perfluorodecanethiol; BRFT, branched fluorinated thiol; SAM, self-assembled monolayer; FSAM, fluorinated self-assembled monolayer; CA, contact angle; CAH, contact angle hysteresis; OWRK, Owens−Wendt−Rabel−Kaelble; AFM, atomic force microscopy; LFM, lateral force microscopy; XPS, X-ray photoelectron spectroscopy; XRR, X-ray reflectivity; SLD, scattering length density; MD, molecular dynamics; RMSD, root-mean-square distance; PDF, pair distribution function

REFERENCES

(1) Scarratt, L. R. J.; Steiner, U.; Neto, C. A review on the mechanical and thermodynamic robustness of superhydrophobic surfaces. *Adv. Colloid Interface Sci.* **2017**, *246* (May), 133−152.

(2) Wen, G.; Guo, Z.; Liu, W. Biomimetic polymeric superhydrophobic surfaces and nanostructures: from fabrication to applications. *Nanoscale* **2017**, *9* (10), 3338−3366.

(3) Chen, L.; Guo, Z.; Liu, W. Outmatching superhydrophobicity: bio-inspired re-entrant curvature for mighty superamphiphobicity in air. *J. Mater. Chem. A* **2017**, *5* (28), 14480−14507.

(4) Vericat, C.; Vela, M. E.; Benitez, G.; Carro, P.; Salvarezza, R. C. Self-assembled monolayers of thiols and dithiols on gold: new challenges for a well-known system. *Chem. Soc. Rev.* **2010**, *39* (5), 1805−1834.

(5) Casalini, S.; Bortolotti, C. A.; Leonardi, F.; Biscarini, F. Self-assembled monolayers in organic electronics. *Chem. Soc. Rev.* **2017**, *46* (1), 40−71.

(6) Zenasni, O.; Jamison, A. C.; Lee, T. R. The impact of fluorination on the structure and properties of self-assembled monolayer films. *Soft Matter* **2013**, *9* (28), 6356−6370.

(7) Krafft, M. P.; Riess, J. G. Per- and polyfluorinated substances (PFASs): Environmental challenges. *Curr. Opin. Colloid Interface Sci.* **2015**, *20*, 192−212.

(8) Dichiarante, V.; Milani, R.; Metrangolo, P. Natural surfactants towards a more sustainable fluorine chemistry. *Green Chem.* **2018**, *20*, 13−27.

(9) Wang, Z.; Cousins, I. T.; Scheringer, M.; Hungerbühler, K. Fluorinated alternatives to long-chain perfluoroalkyl carboxylic acids (PFCAs), perfluoroalkane sulfonic acids (PFSAs) and their potential precursors. *Environ. Int.* **2013**, *60* (2013), 242−248.

(10) Li, Q.; Yan, Y.; Yu, M.; Song, B.; Shi, S.; Gong, Y. Synthesis of polymeric fluorinated sol-gel precursor for fabrication of superhydrophobic coating. *Appl. Surf. Sci.* **2016**, *367*, 101−108.

(11) Schuster, T.; Krumpfer, J. W.; Schellenberger, S.; Friedrich, R.; Klapper, M.; Müllen, K. Effects of chemical structure on the dynamic and static surface tensions of short-chain, multi-arm nonionic fluorosurfactants. *J. Colloid Interface Sci.* **2014**, *428*, 276−285.

(12) Ramos Chagas, G.; Darmanin, T.; Godeau, G.; Amigoni, S.; Guittard, F. Superhydrophobic properties of electrodeposited fluorinated polypyrenes. *J. Fluorine Chem.* **2017**, *193*, 73−81.

(13) Darmanin, T.; Tarrade, J.; Celia, E.; Guittard, F. Superoleophobic meshes with high adhesion by electrodeposition of conducting polymer containing short perfluorobutyl chains. *J. Phys. Chem. C* **2014**, *118* (4), 2052−2057.

(14) Bellanger, H.; Darmanin, T.; Taffin de Givenchy, E.; Guittard, F. Influence of intrinsic oleophobicity and surface structuration on the superoleophobic properties of PEDOP films bearing two fluorinated tails. *J. Mater. Chem. A* **2013**, *1* (8), 2896−2903.

(15) Darmanin, T.; Guittard, F. Enhancement of the superoleophobic properties of fluorinated PEDOP using polar glycol spacers. *J. Phys. Chem. C* **2014**, *118* (46), 26912−26920.

(16) Bellanger, H.; Darmanin, T.; de Givenchy, E. T.; Guittard, F. Influence of long alkyl spacers in the elaboration of superoleophobic surfaces with short fluorinated chains. *RSC Adv.* **2013**, *3* (16), 5556−5562.

(17) Darmanin, T.; Guittard, F. Superoleophobic surfaces with short fluorinated chains? *Soft Matter* **2013**, *9* (25), 5982−5990.

(18) Jiang, J.; Zhang, G.; Wang, Q.; Zhang, Q.; Zhan, X.; Chen, F. Novel Fluorinated Polymers Containing Short Perfluorobutyl Side Chains and Their Super Wetting Performance on Diverse Substrates. *ACS Appl. Mater. Interfaces* **2016**, *8* (16), 10513−10523.

(19) El-Maiss, J.; Darmanin, T.; Guittard, F. Branched versus linear perfluorocarbon chains in the formation of superhydrophobic electrodeposited films with low bioaccumulative potential. *J. Mater. Sci.* **2014**, *49* (22), 7760−7769.

(20) Tirotta, I.; Mastropietro, A.; Cordiglieri, C.; Gazzera, L.; Baggi, F.; Baselli, G.; Grazia Bruzzone, M.; Zucca, I.; Cavallo, G.; Terraneo, G.; et al. A superfluorinated molecular probe for highly sensitive in vivo ^{19}F-MRI. *J. Am. Chem. Soc.* **2014**, *136* (24), 8524−8527.

(21) Dichiarante, V.; Tirotta, I.; Catalano, L.; Terraneo, G.; Raffaini, G.; Chierotti, M. R.; Gobetto, R.; Baldelli Bombelli, F.; Metrangolo, P. Superfluorinated and NIR-luminescent gold nanoclusters. *Chem. Commun.* **2017**, *53* (3), 621−624.

(22) Larmour, I. A.; Bell, S. E. J.; Saunders, G. C. Remarkably simple fabrication of superhydrophobic surfaces using electroless galvanic deposition. *Angew. Chem., Int. Ed.* **2007**, *46* (10), 1710−1712.

(23) Kaelble, D. H. Dispersion-Polar Surface Tension Properties of Organic Solids. *J. Adhes.* **1970**, *2*, 66−81.

(24) Owens, D. K.; Wendt, R. C. Estimation of the surface free energy of polymers. *J. Appl. Polym. Sci.* **1969**, *13*, 1741−1747.

(25) Timonen, J. V. I; Latikka, M.; Ikkala, O.; Ras, R. H. A. Free-decay and resonant methods for investigating the fundamental limit of superhydrophobicity. *Nat. Commun.* **2013**, *4* (4), 1−8.

(26) Raffaini, G.; Ganazzoli, F. Protein adsorption on biomaterial and nanomaterial surfaces: a molecular modeling approach to study non-covalent interactions. *J. Appl. Biomater. Funtional Mater.* **2010**, *8* (3), 135−145.

(27) Milionis, A.; Dang, K.; Prato, M.; Loth, E.; Bayer, I. S. Liquid repellent nanocomposites obtained from one-step water-based spray. *J. Mater. Chem. A* **2015**, *3*, 12880−12889.

(28) Hamoudi, H.; Prato, M.; Dablemont, C.; Cavalleri, O.; Canepa, M.; Esaulov, V. A. Self-Assembly of 1,4-Benzenedimethanethiol Self-Assembled Monolayers on Gold. *Langmuir* **2010**, *26* (10), 7242−7247.

(29) Cavalleri, O.; Gonella, G.; Terreni, S.; Vignolo, M.; Floreano, L.; Morgante, A.; Canepa, M.; Rolandi, R. High resolution X-ray photoelectron spectroscopy of L-cysteine self-assembled films. *Phys. Chem. Chem. Phys.* **2004**, *6*, 4042−4046.

(30) Barriet, D.; Lee, T. R. Fluorinated self-assembled monolayers: composition, structure and interfacial properties. *Curr. Opin. Colloid Interface Sci.* **2003**, *8*, 236−242.

(31) Naud, C.; Calas, P.; Commeyras, A. Critical influence of the fluorinated chain length in the self-assembly of terminally perfluorinated alkanethiol monolayers on gold surfaces. An electrochemical study. *Langmuir* **2001**, *17* (16), 4851−4857.

(32) Mougin, K.; Haidara, H. Nanoscale Friction of Self-assembled Monolayers. In *Fundamentals of Friction and Wear on the Nanoscale*; Meyer, E., Gnecco, E., Eds.; Springer, Berlin, Heidelberg, 2007; pp 619−645, DOI: 10.1007/978-3-540-36807-6_28.

(33) Genzer, J.; Efimenko, K. Creating Long-Lived Superhydrophobic Polymer Surfaces Through Mechanically Assembled Monolayers. *Science* **2000**, *290* (5499), 2130−2133.

(34) Patois, T.; Et Taouil, A.; Lallemand, F.; Carpentier, L.; Roizard, X.; Hihn, J.-Y.; Bondeau-Patissier, V.; Mekhalif, Z. Microtribological and corrosion behaviors of 1H,1H,2H,2H-perfluorodecanethiol self-assembled films on copper surfaces. *Surf. Coat. Technol.* **2010**, *205*, 2511−2517.

(35) Qiao, S.; Li, S.; Li, Q.; Li, B.; Liu, K.; Feng, X. Q. Friction of Droplets Sliding on Microstructured Superhydrophobic Surfaces. *Langmuir* **2017**, *33* (47), 13480−13489.
(36) Chu, Z.; Seeger, S. Superamphiphobic surfaces. *Chem. Soc. Rev.* **2014**, *43* (8), 2784−2798.
(37) Lee, H. J.; Jamison, A. C.; Lee, T. R. Surface Dipoles: A Growing Body of Evidence Supports Their Impact and Importance. *Acc. Chem. Res.* **2015**, *48*, 3007−3015.
(38) Wu, X.; Liu, M.; Zhong, X.; Liu, G.; Wyman, I.; Wang, Z.; Wu, Y.; Yang, H.; Wang, J. Smooth Water-Based Antismudge Coatings for Various Substrates. *ACS Sustainable Chem. Eng.* **2017**, *5* (3), 2605−2613.
(39) Colorado, R.; Lee, T. R. Wettabilities of self-assembled monolayers on gold generated from progressively fluorinated alkanethiols. *Langmuir* **2003**, *19* (8), 3288−3296.
(40) Nishino, T.; Meguro, M.; Nakamae, K.; Matsushita, M.; Ueda, Y. The Lowest Surface Free Energy Based on $-CF_3$ Alignment. *Langmuir* **1999**, *15* (13), 4321−4323.
(41) Good, R. J. Contact angle, wetting, and adhesion: a critical review. *J. Adhes. Sci. Technol.* **1992**, *6* (12), 1269−1302.